Inorganic Chemistry
Cite This: Inorg. Chem. 2019, 58, 14420−14428
Article
pubs.acs.org/IC

Synthesis, Magnetic and High-Field EPR Investigation of Two Tetranuclear Ni^{II}-Based Complexes

Lívia B. L. Escobar,[†,‡] Guilherme P. Guedes,[†] Stéphane Soriano,[§] Jonathan Marbey,[‡,∥] Stephen Hill,*[,‡,∥] Miguel A. Novak,[⊥] and Maria G. F. Vaz*[,†]

[†]Instituto de Química, Universidade Federal Fluminense, Niterói, Rio de Janeiro 24020-141, Brazil
[‡]NHMFL, Florida State University, Tallahassee, Florida 32310, United States
[§]Instituto de Física, Universidade Federal Fluminense, Niterói, Rio de Janeiro 24210-346, Brazil
[∥]Department of Physics, Florida State University, Tallahassee, Florida 32306, United States
[⊥]Instituto de Física, Universidade Federal do Rio de Janeiro, Rio de Janeiro, 21941-972, Brazil

Supporting Information

ABSTRACT: Two tetranuclear compounds with a cubane-like structure were synthesized from a one-pot reaction between Ni^{II} and 2,2,6,6-tetramethyl-3,5-heptanedione (Hdpm) for **1** or 4,4,4-trifluoro-1-phenyl-1,3-butanedione (Hbta) for **2** in the presence of sodium methoxide. The crystal structures of both compounds have been determined by single-crystal X-ray diffraction, and their magnetic properties have been studied by SQUID magnetometry as well as by high-field electron paramagnetic resonance (HFEPR) spectroscopy. For **1**, the temperature dependence of the magnetic susceptibility can be fitted by taking into account Ni···Ni ferromagnetic interactions, which leads to an $S = 4$ ground-state spin. For **2**, both antiferromagnetic and ferromagnetic interactions are present. However, the latter are dominant, which also leads to an $S = 4$ ground-state spin, in good agreement with the HFEPR study.

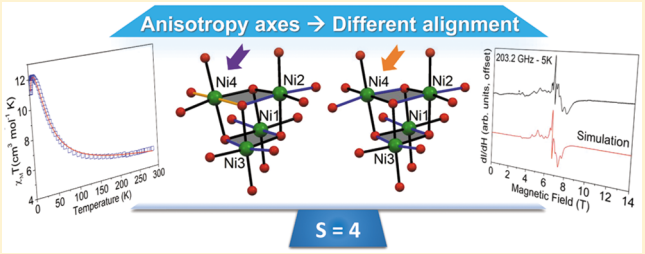

INTRODUCTION

The initial discovery of slow relaxation of magnetization in a Mn_{12} cluster triggered intense research activity in the field of molecular magnetism.[1−3] Since then, there have been widespread efforts to obtain magnetically bistable molecular complexes, also known as single-molecule magnets (SMMs), that can exhibit magnetization blocking at readily accessible temperatures to be utilized in novel applications such as information storage, spintronics, quantum computing, etc.[4,5]

Among SMMs, compounds containing a tetranuclear Ni−O−Ni bridged cubane-like core have been intensively studied.[6−9] The magnetic properties of these Ni^{II} cubane complexes depend on various factors, such as the nature of the ligands, the coordination numbers and geometries of the metal centers, and other structural parameters such as the Ni−O−Ni bond angles and distances. Changes to the local coordination of the Ni^{II} ions can significantly affect the magnetic behavior, both through zero-field splitting (ZFS) anisotropy associated with the individual Ni^{II} sites and the exchange coupling between them.[10] For these types of compounds, a correlation between the sign and magnitude of the magnetic exchange constant (J) and key structural parameters has been established.[8]

One of the strategies for the creation of new cubane complexes is the use of β-diketonates, a widely exploited ligand in molecular magnetism.[11] In a previous article,[12] some of us described the influence of small ligand changes on the magnetic properties of two Co^{II} cubane compounds. Substitution of the ethanol molecules in $[Co_4(tta)_4(MeO)_4(EtOH)_4]$ with methanol distorts the Co^{II} coordination spheres, resulting in subtle changes to the bridging angles, leading to a significant change in magnetic behavior. Additionally, these complexes can be used to create structures with larger nuclearity. For example, the reaction of tetranuclear cubanes with different alcohol molecules, such as isopropanol or n-butanol, can furnish heptanuclear complexes.[13] Since ferromagnetic interactions are dominant in such compounds, they are promising candidates for SMMs.

High-frequency electron paramagnetic resonance (HFEPR) represents a powerful tool in the spectroscopic investigation of coordination complexes of paramagnetic transition-metal ions that are not amenable to study by conventional EPR (frequencies up to 35 GHz and magnetic fields up to 2 T).[14,15] One of the most important advantages of using HFEPR spectroscopy is associated with the investigation of the ZFS parameters of highly anisotropic metal ions.[16] In this work, we are using this technique to understand the magnetic properties of Ni^{II} cubane-like complexes containing β-diketones ligands. Compound **1** was obtained using the β-

Received: June 18, 2019
Published: October 18, 2019

DOI: 10.1021/acs.inorgchem.9b01816
Inorg. Chem. 2019, 58, 14420−14428

diketonate ligand 2,2,6,6-tetramethyl-3,5-heptanedione (Hdpm), while **2** was synthesized by using 4,4,4-trifluoro-1-phenyl-1,3-butanedione (Hbta) (Scheme 1). For both compounds, ferromagnetic interactions are dominant, leading to high-spin ground states with $S = 4$, as confirmed by the HFEPR studies.

Scheme 1. Structures of the β-Diketone Ligands

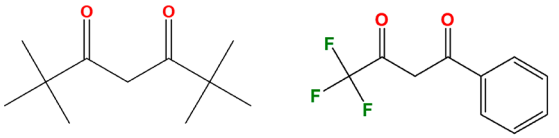

2,2,6,6-tetramethyl-3,5-heptanodione (Hdpm) | 4,4,4-trifluoro-1-phenyl-1,3-butanedione (Hbta)

EXPERIMENTAL SECTION

Preparation. All reagents and solvents were purchased from commercial sources and used without further purification. First, 0.620 g (3.39 mmol) of $[Ni(NO_3)_2]\cdot 6H_2O$ and 3.39 mmol of the β-diketonate ligand, 2,2,6,6-tetramethyl-3,5-heptanedione (Hdpm) for **1** or 4,4,4-trifluoro-1-phenyl-1,3-butanedione (Hbta) for **2**, were dissolved in 20 mL of dried methanol (Scheme 2). The light green solutions were stirred for 30 min; then, 120 μL of a 30% (m/v) sodium methoxide solution was added, and green solids were formed. The mixtures were stirred for one additional hour and filtered off. The crude products were dissolved in 30 mL of diethyl ether and filtered to remove any insoluble material. Single crystals were obtained after 2−3 days by slow diffusion of methanol vapors into diethyl ether solution. Powder X-ray diffraction patterns for compounds **1** and **2** were compared with the simulated ones, predicted from the single-crystal XRD. The experimental and simulated powder XRD patterns corresponded well in peak positions and relative intensities, confirming the crystalline phase purity of the compounds (see Figure S1 in the SI for details).

*$[Ni_4(dpm)_4(MeO)_4(MeOH)_4]$ (**1**).* Yield: 0.727 g (75%). IR (ν/cm^{-1}): 3275, 2955, 2916, 2812, 1589, 1410, 1220, 1136. Anal. calcd for $C_{52}H_{104}Ni_4O_{16}$: C, 51.19; H, 8.59%. Found: C, 49.58; H, 8.39%.

*$[Ni_4(bta)_4(MeO)_4(MeOH)_4]$ (**2**).* Yield: 0.650 g (58%). IR (ν/cm^{-1}): 3068, 2930, 2818, 1627, 1578, 1492, 1290. While crystallography shows the presence of one crystallization ethyl ether solvent molecule in the lattice of compound **2**, microanalysis was more consistent with the ethyl ether free elemental formula, suggesting a ready loss of the ethyl ether when the single crystals were removed from the mother liquor and opened to air. Anal. calcd for $C_{48}H_{57}F_{12}Ni_4O_{16}$: C, 42.78; H, 3.89%. Found: C, 42.86; H, 3.90%.

The elemental analyses (CHN) were carried out on a PerkinElmer 2400 Series II analyzer. Powder X-ray diffraction data for both samples were collected on a Bruker D8 Advance equipped with a LynxEye detector at room temperature. Single-crystal X-ray diffraction data were obtained at room temperature with an Oxford GEMINI A Ultra diffractometer for **1** and with a Bruker−Nonius KAPPA-CCD diffractometer for **2**, both using graphite monochromated Mo-$K\alpha$ radiation (λ = 0.71069 Å). For compound **1**, data collection, reduction, and cell refinement were performed by CRYSALIS RED (Oxford Diffraction Ltd., v. 1.171.32.38).[17] For compound **2**, final unit cell parameters were based on the fitting of the positions of all reflections using COLLECT.[18] The data integration and scaling of the reflections were performed with the HKL SCALEPACK.[19] Empirical multiscan absorption corrections using equivalent reflections were performed with the program SORTAV.[20] Both crystal structures were solved and refined using SHELXS and SHELXL packages.[21] Compounds **1** and **2** presented disorder in the methyl groups, trifluoromethyl or phenyl groups, which was modeled considering two possible arrangements. The structures were drawn using the ORTEP-3 for WINDOWS[22] and VESTA programs.[23] Summaries of the crystal data, data collection, and refinement for compounds **1** and **2** are listed in Table 1. Selected bond lengths and bond angles are summarized in Table S1. Figure S2 shows the ORTEP representations of the asymmetric units for compounds **1** and **2**.

Table 1. Summary of the Crystal Structure, Data Collection, and Refinement for 1 and 2

	1	2
chemical formula	$C_{52}H_{104}Ni_4O_{16}$	$2\cdot(C_{48}H_{57}F_{12}Ni_4O_{16})C_4H_{10}O$
formula mass	1220.19	2769.44
crystal system	monoclinic	triclinic
space group	$P2_1/n$	$P\bar{1}$
radiation type	Mo Kα	Mo Kα
temperature/K	293 K	293 K
a/Å	13.1816(4)	14.6770(4)
b/Å	30.7361(8)	20.5450(3)
c/Å	15.9205(4)	23.0590(4)
α/deg	90.00	64.154(1)
β/deg	93.145(2)	80.434(1)
γ/deg	90.00	78.594(1)
V/Å^3	6440.5(3)	6108.81(16)
Z	4	4
ρ (calculated), (Mg m^{-3})	1.258	1.497
μ/mm^{-1}	1.21	1.31
no. of reflections measured	60647	35640
no. of independent reflections	11379	21494
θ range/deg	1.84−25.03	4.10−25.10
index range	$h = -15 \rightarrow 15$	$h = -17 \rightarrow 16$
	$k = -36 \rightarrow 36$	$k = -24 \rightarrow 24$
	$l = -18 \rightarrow 18$	$l = -27 \rightarrow 26$
R_{int}	0.059	0.021
final R_1 values ($I > 2\sigma(I)$)	0.058	0.073
final $wR(F^2)$ values ($I > 2\sigma(I)$)	0.150	0.223
final R_1 values (all data)	0.080	0.098
final $wR(F^2)$ values (all data)	0.166	0.197
goodness of fit on F^2	1.04	1.03
CCDC	1903092	1903630

Magnetic Measurements. DC magnetic measurements were performed on a Cryogenic Sx600 SQUID magnetometer in the temperature range of 2−280 K. The powder samples were pressed and placed in a gelatin capsule, and the diamagnetic contribution of the sample and holder was taken into account. The sample's diamagnetism correction was estimated from Pascal's constants.[24]

Scheme 2. Synthesis of the Tetranuclear Ni^{II}-Based Complexes

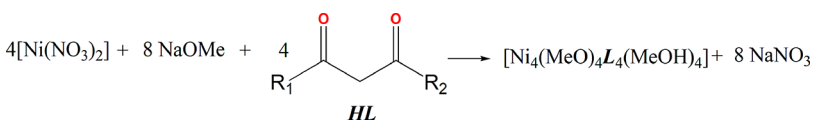

DOI: 10.1021/acs.inorgchem.9b01816
Inorg. Chem. 2019, 58, 14420−14428

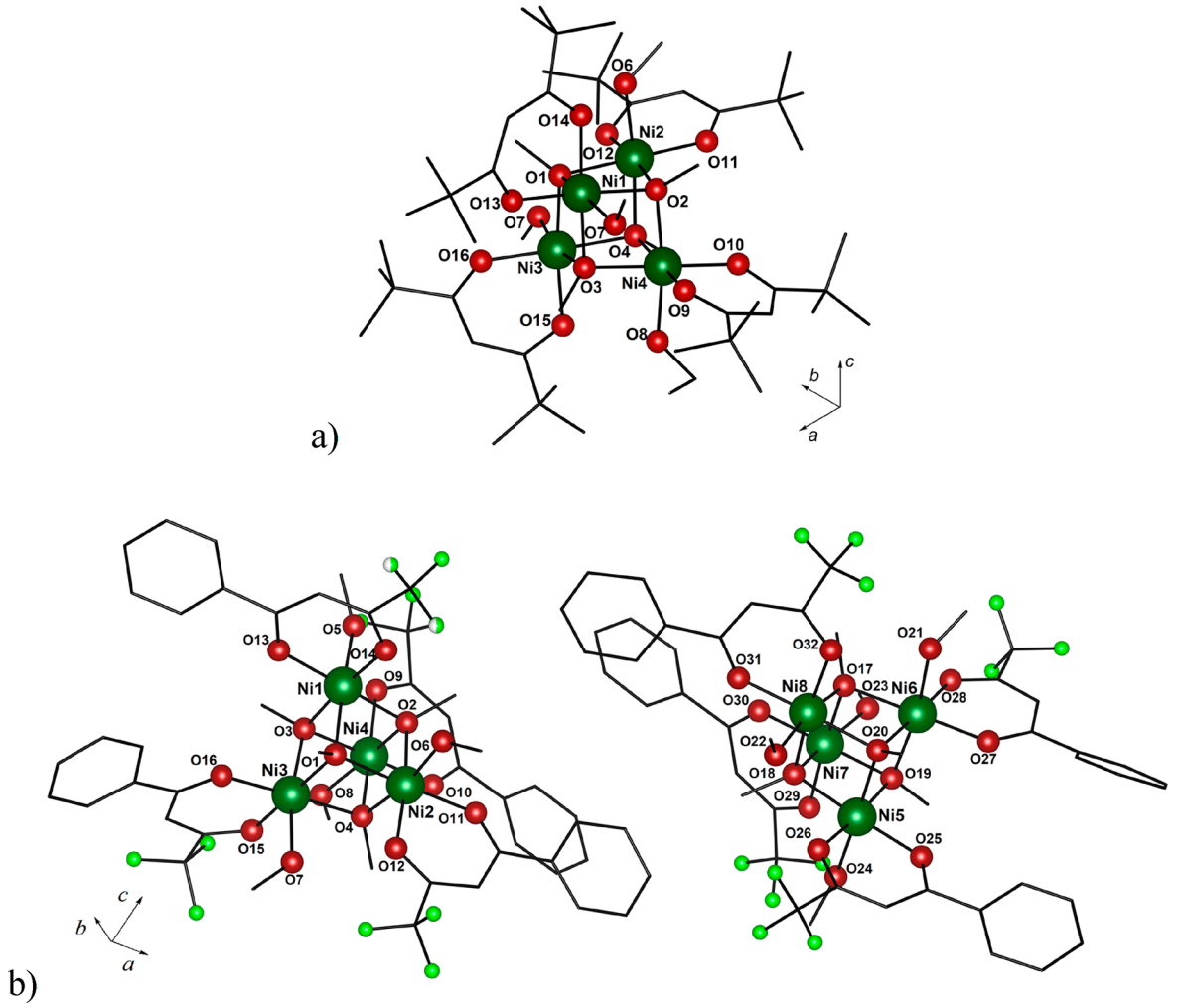

Figure 1. Asymmetric unit of compounds **1** (a) and **2** (b). Hydrogen atoms, part of the disordered groups, as well as the ethyl ether molecule were omitted for the sake of clarity. Colors: dark green = nickel, red = oxygen, light green = fluorine, black = carbon.

HFEPR Spectroscopy. High-field, high-frequency EPR measurements were carried out at the U.S. National High Magnetic Field Laboratory (NHMFL), in Tallahassee, Florida, on powder samples of compounds **1** and **2**. The powder spectra were recorded at temperatures ranging from 5 K to 20 K on a home-built spectrometer at the EMR facility of the NHMFL.[25] The instrument is a transmission-type device in which microwaves are propagated in cylindrical lightpipes. The microwaves are generated by a phase-locked Virginia Diodes source generating frequencies in the range of 25−628.8 GHz. A superconducting magnet (Oxford Instruments) capable of reaching a field of 17 T was employed. The pure powder samples were obtained by grinding single crystals, which were then constrained to prevent magnetic torquing at high magnetic fields. All simulations of powder EPR spectra were performed using the EasySpin software.[26]

RESULTS AND DISCUSSION

Synthesis of Tetranuclear Complexes with Cubane-like Structures. The procedure used to obtain complexes **1** and **2** was adapted from the one used for the preparation of tetranuclear Co^{II}-based cubanes.[12] The differences consist of the replacement of $CoCl_2$ with $Ni(NO_3)_2$ and the change of the β-diketonate (4,4,4-trifluoro-1-(2-thienyl)-1,3-butanedione (Htta). Thus, two complexes with cubane-like structures were obtained by a one-pot reaction, in which $Ni(NO_3)_2$ reacted with 2,2,6,6-tetramethyl-3,5-heptanedione (Hdpm) or 4,4,4-trifluoro-1-phenyl-1,3-butanedione (Hbta) in the presence of sodium methoxide to afford **1** and **2**, respectively (Scheme 2).

There exist alternative methodologies of obtaining Ni^{II} derivatives displaying the general formula $[Ni_4(OMe)_4(diketonate)_4(MeOH)_4]$ that require different starting metal precursors and diketonate ligands than what is discussed here. In regards to the equimolar reaction of nickel(II) acetate, the initially prepared Na(dbm) salt (Hdbm = dibenzoylmethane) and NaOH in MeOH can lead to a $[Ni_4(OMe)_4(dbm)_4(MeOH)_4]$ complex. By utilizing the same synthetic route, the isostructural nickel and cobalt derivatives with the acetylacetonate ligand $[M_4(acac)_4(OMe)_4(MeOH)_4]$ can be obtained.[27] Some authors have previously explored the alcoholysis methodology to prepare compounds containing β-diketonates with electron-withdrawing groups such as the hexafluoroacetonate ligand. Other researchers reported the use of $[Ni(hfac)_2]\cdot 2H_2O$ as a metal precursor, instead of acetate or nitrate salts. In this methodology, a methanolic solution of sodium hydroxide and $[Ni(hfac)_2]\cdot 2H_2O$ is heated to reflux, and single-crystals are collected after a couple of days. A similar approach using alcoholysis of $[Co(\beta\text{-diketonate})_2]$ precursors in the presence of strong bases also leads to $[Co_4(OMe)_4(\beta\text{-diketonate})_4(MeOH)_4]$.[12] The synthetic procedure used in this work for **1** and **2** greatly simplifies the chemical manipulations in comparison to the compounds discussed

DOI: 10.1021/acs.inorgchem.9b01816
Inorg. Chem. 2019, 58, 14420−14428

above. Here, we avoid the preparation of metal complex precursors or diketonate salts and allow a one-pot approach at room temperature. This procedure is also applicable to β-diketonate ligands with different substituents and basicity; the Hdpm contains strong electron-donating groups, two *tert*-butyl, while Hbta has phenyl and trifluoromethyl as electron-withdrawing ones. The same synthetic route exploited here can be used to obtain complexes with other metal ions. Depending on the chosen metal ion, compounds with higher nuclearity can be formed.[28]

Crystal Structures. Compound **1** crystallizes in the $P2_1/n$ monoclinic space group with one molecule in the asymmetric unit, which is shown in Figure 1(a). The molecule has a cuboidal Ni_4O_4 core with the four octahedrally coordinated Ni^{II} atoms occupying four alternating corners of the cube. The other corners are occupied by oxygen atoms of methoxide groups (O4, O5, O6, and O7). The overall arrangement has an approximate S_4 symmetry. This compound is isomorphic to the complex $[Co_4(dpm)_4(MeO)_4(MeOH)_4]$ reported previously by Berry and co-workers in 2004.[29] In this arrangement, the symmetries of the metal ions and bridging atoms have also been seen in other tetranuclear clusters such as $[Ni_4(hfac)_4(MeO)_4(MeOH)_4]$[30] and $[Ni_4(MeO)_4(O_2CAr^{Tol})_4(MeOH)_6]\cdot 1.5\ (MeOH)$.[6]

In compound **1** the average distance between the Ni^{II} ions is 3.09(1) Å. The cube formed by the four Ni^{II} and oxygen atoms is distorted, with all O−Ni−O angles smaller than 90°, while all Ni−O−Ni angles are greater than 90°. The faces of the cubane core of compound **1** may be grouped into two distinct sets, i.e., the first represented by two parallel faces with Ni−O−Ni bond angles close to 99°, with the other four having a mean angle of 96.5(1)°, as seen in Figure 2(a). To furnish a complete octahedral coordination environment, each Ni^{II} ion is also bonded to a CH_3OH molecule (O3, O14, O15, and O16) and chelated by a dpm ligand. The crystal packing of this compound is stabilized by weak interactions between the methyl groups of the dpm ligands.

Figure 1(b) shows the asymmetric unit of compound **2**, which consists of two tetranuclear Ni^{II} units and one crystallization ethyl ether solvent molecule. Complex **2** has two cuboidal Ni_4O_4 cores, with the four octahedrally coordinated Ni^{II} ions occupying four alternating corners of a cube. The other corners are occupied by oxygen atoms of methoxide groups. The coordination sphere of each metal ion is completed by a bta ligand and a methanol molecule, leading to a distorted octahedral geometry. Selected bond angles and bond lengths for both compounds are given in Table S1. It is important to highlight that the average bond length of the methoxide bridges, $Ni-O_{methoxide}$, is similar to those observed in the tetranuclear compounds $[Ni_4(hfac)_4(MeO)_4(MeOH)_4]$ and $[Ni_4(MeO)_4(dbm)_4(MeOH)_4]$ (hfac = hexafluoroacetylacetonate and dbm = dibenzoylmethanoate) reported previously.[30,31]

Similar to complex **1**, the Ni_4O_4 cubane cores in **2** are distorted due to the Ni−O−Ni bond angles ranging from 95° to 99°. The presence of two distinct sets of faces is again evident for each cubane core within the asymmetric unit, i.e., the first represented by two parallel faces with Ni−O−Ni bond angles close to 99°, and the other by four faces with bond angles ranging from 95° to 97° (see Figure 2(b) and Table S1). Regarding the intramolecular Ni···Ni distances, two are somewhat longer at approximately 3.100 Å, while the other four are shorter with values around 3.060 Å. Intermolecular

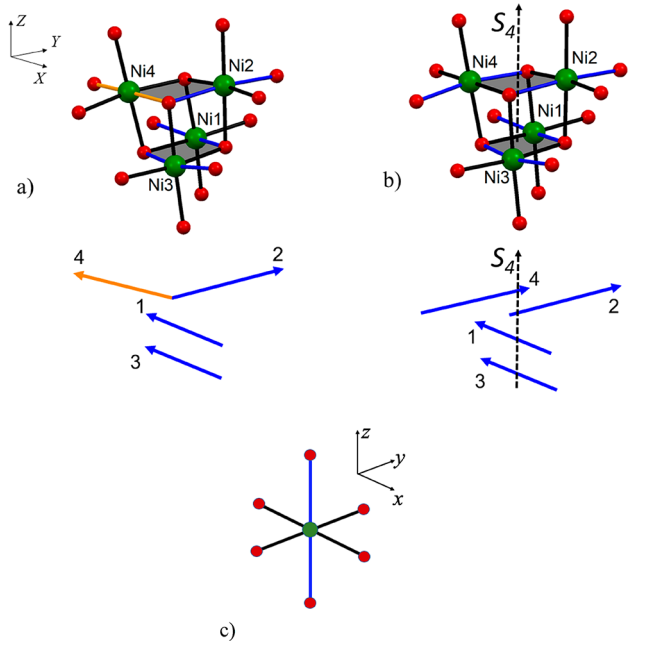

Figure 2. Arrangement of local Ni−O elongation axes (blue/orange lines) in **1** (a) and **2** (b); the pseudo-S_4 axis is shown in dashed lines, and the second cubane unit of compound **2** has been omitted for the sake of clarity. Complex **1** presents a different elongation axis alignment (orange line) for Ni4 when compared with the same ion in complex **2**. The shaded surfaces represent cube faces with Ni−O−Ni angles close to 99°. (c) The orientation of the local coordination axes for each metal ion in compounds **1** and **2** used to calculate the d_{str} value shown in Table 2.

hydrogen bonds between the methanol molecule, the oxygen atoms, and the trifluoromethyl group from the β-diketonate ligand are present in the crystal packing of complex **2**.

Recent investigations of families of centrosymmetric MX_6 octahedral complexes (M = metal ion, X = coordinating atom) have established clear magnetostructural correlations between the single-ion axial ZFS parameter, D, and the tetragonal distortion parameter defined as[32−34]

$$d_{str} = d_z - \frac{1}{2}(d_x + d_y) \quad (1)$$

where d_x, d_y, d_z are the M−X bond lengths along the local x, y, and z directions. The parameter d_{str} characterizes the degree of axial compression/elongation of the octahedral coordination environment around the metal center, although the expression applies equally to rhombic cases with three sets of M−X distances. The two most similar distances, d_x and d_y, define the equatorial plane of the complex while the axial positions are defined by d_z [see Figure 2(c)]. As such, a positive (negative) d_{str} signifies an axially elongated (compressed) tetragonal bipyramid. Although essentially no symmetry is present at the Ni^{II} sites in **1** and **2**, the geometry is reasonably close to octahedral. We therefore compute d_{str} for each ion by taking the average distance for each pair of Ni−O bonds aligned approximately along the three Cartesian axes [see Figure 2(c)], again with the two most similar distances corresponding to d_x and d_y. Based on this analysis, the coordination geometry corresponds to an elongated tetragonal bipyramid in all cases for complexes **1** and **2** (see Table 2) which, according to Boča et al.,[32,34] signifies positive ZFS D parameters.

DOI: 10.1021/acs.inorgchem.9b01816
Inorg. Chem. 2019, 58, 14420−14428

Table 2. Tetragonal Distortion Parameters, d_{str}, at Each Ni^{II} Site for the Two Complexes

complex **1**		complex **2**			
ion	d_{str} (pm)	ion	d_{str}	ion	d_{str} (pm)
Ni1	+4.35	Ni1	+3.50	Ni5	+6.07
Ni2	+2.40	Ni2	+3.67	Ni6	+3.35
Ni3	+5.75	Ni3	+4.60	Ni7	+5.92
Ni4	+5.05	Ni4	+4.00	Ni8	+4.80

Figure 2 shows the arrangement of the local hard axes (elongated bonds shown in blue and orange) for each Ni^{II} ion in compounds **1** and **2**, with the shaded surfaces representing faces with Ni−O−Ni angles close to 99°. As can be seen, the Ni_4O_4 cube has approximate S_4 symmetry in the case of compound **2**. However, this is not the case in compound **1**, where the elongation axis for the ion labeled Ni4 is highlighted in orange to emphasize its distinct orientation in comparison to the same ion in complex **2**.

The magnetic exchange interactions between Ni^{II} ions through the methoxo bridges are very sensitive to the Ni−O−Ni angles.[10] Meanwhile, local distortions of the coordination geometries at each metal site govern the magnetic anisotropy associated with each Ni^{II} ion,[34] where, in the present case, an elongation ($d_{str} > 0$) of the octahedral coordination sphere leads to a local easy-plane anisotropy, with a positive $D_{Ni^{II}}$ parameter and local hard-axes defined by the elongated Ni−O contacts (represented by the blue/orange bonds in Figures 2(a) and (b)).[35] Looking carefully at the structure of the cubane core of complex **2** (Figure 2(b)), one observes parallel hard-axis alignments on each of the shaded faces, with the top face rotated ∼90° with respect to the bottom face about the molecular *Z*-axis. This arrangement corresponds to an approximate S_4 molecular symmetry, suggesting that the ZFS tensor for compound **2** should be quite axial.[9,36] By contrast, the hard axis alignments for complex **1** (Figure 2a) suggest a ZFS tensor with lower symmetry.

Magnetic Properties. The magnetic properties of compounds **1** and **2** have been investigated in the temperature range of 2−300 K. The plots of $\chi_M T$ versus T, where χ_M is the molar magnetic susceptibility, are shown in Figure 3. The χ_MT values at the highest temperatures are 5.3 $cm^3\ mol^{-1}$ K for **1** and 5.6 $cm^3\ mol^{-1}$ K for **2**, which are higher than expected for four noninteracting Ni^{II} ions with $S = 1$ and $g = 2.0$ (χ_MT = 4.0 $cm^3\ mol^{-1}$ K). For both compounds, χ_MT increases steadily as the temperature is lowered, indicating the presence of ferromagnetic interactions between the spin centers. It reaches maximum values of 12.1 $cm^3\ mol^{-1}$ K at 8.1 K for **1** and 12.0 $cm^3\ mol^{-1}$ K at 8.2 K for **2**. These relatively high χ_MT maxima were observed for similar Ni^{II}-based cubanes.[10,37] Subsequently, upon lowering the temperature, χ_MT decreases due to antiferromagnetic intermolecular interactions and/or magnetic anisotropy (ZFS) associated with the Ni^{II} ions.

As discussed previously in the crystal structure section, two sets of cube faces with different Ni−O−Ni angles are notably present in these compounds: one set of four faces with Ni−O−Ni angles around 96.5°, and another one of two faces with angles around 99° [shaded surfaces in Figures 2(a) and (b)]. Therefore, two different coupling constants J_1 and J_2 were considered in the analysis of the magnetic data, and the following spin Hamiltonian was used for compound **2**:

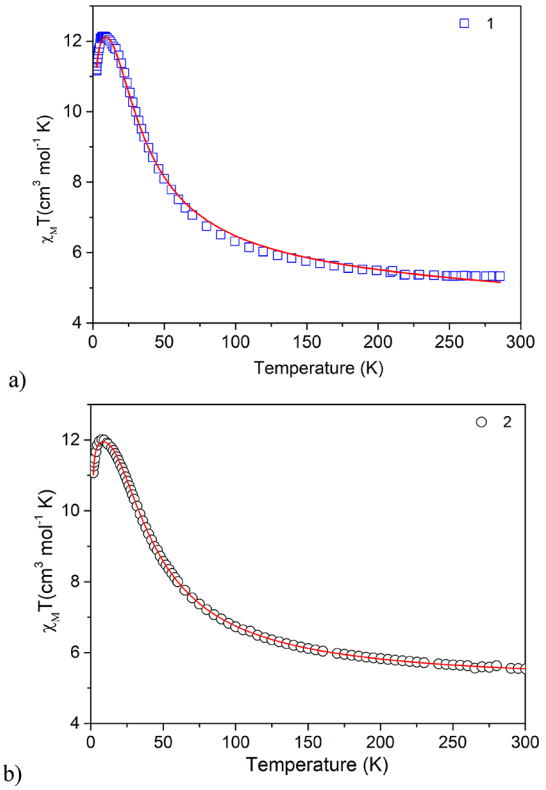

Figure 3. Temperature dependence of the dc $\chi_M T$ values for powder samples of compounds **1** (a) and **2** (b) measured at a constant magnetic field of 1000 Oe. The red lines correspond to the best fits (vide text).

$$\hat{H} = -J_1(\vec{S}_1\cdot\vec{S}_3 + \vec{S}_2\cdot\vec{S}_4) - J_2(\vec{S}_1\cdot\vec{S}_2 + \vec{S}_2\cdot\vec{S}_3 + \vec{S}_3\cdot\vec{S}_4 + \vec{S}_1\cdot\vec{S}_4) + D(S_{1X}^2 + S_{2Y}^2 + S_{3X}^2 + S_{4Y}^2) + \sum_{i=1}^{4}\mu_B g\vec{B}\cdot\hat{S}_i \quad (2)$$

In order to avoid further overparameterization, we considered the same magnetic interactions (exchange and anisotropy) for both units in **2** and the same ZFS $D_{Ni^{II}}$ parameter for all Ni^{II} ions. In particular, the third term of the Hamiltonian corresponds to the axial ZFS interaction, taking into account the orthogonal arrangements of the local hard axes (see Figure 2b). Using the MagProp routine in the DAVE software suite,[38] the best fit was obtained with $g = 2.19 \pm 0.01$, $J_1 = -1.1 \pm 0.3$ cm^{-1}, $J_2 = 19.6 \pm 0.3$ cm^{-1}, and $D_{Ni^{II}} = +5.2 \pm 0.1$ cm^{-1} (Figure 3b). The magnetic exchange parameters are consistent with similar Ni^{II} oxo-bridged clusters in the literature.[6,39] Indeed, a linear correlation between the exchange constant J and the Ni−O−Ni angle was suggested in earlier studies, with a ferromagnetic interaction for angles less than 99° and an antiferromagnetic interaction for angles greater than 99°.[8,30] However, several other parameters can influence the magnetic exchange constants, such as the nature of the bridge, the Ni−Ni distance, dihedral angles, etc.[10] In our model, J_1 is related to faces with Ni−O−Ni angles around 99° and, therefore, a weak ferro or antiferromagnetic interaction is expected. In contrast, J_2 corresponds to angles around 96.5°, leading to stronger ferromagnetic interactions and to a stabilization of a $S = 4$ spin ground state for the cluster. Finally, the magnitude and sign of the obtained axial ZFS parameter for each Ni^{II} ion lies within the range (from +0.9

DOI: 10.1021/acs.inorgchem.9b01816
Inorg. Chem. 2019, 58, 14420−14428

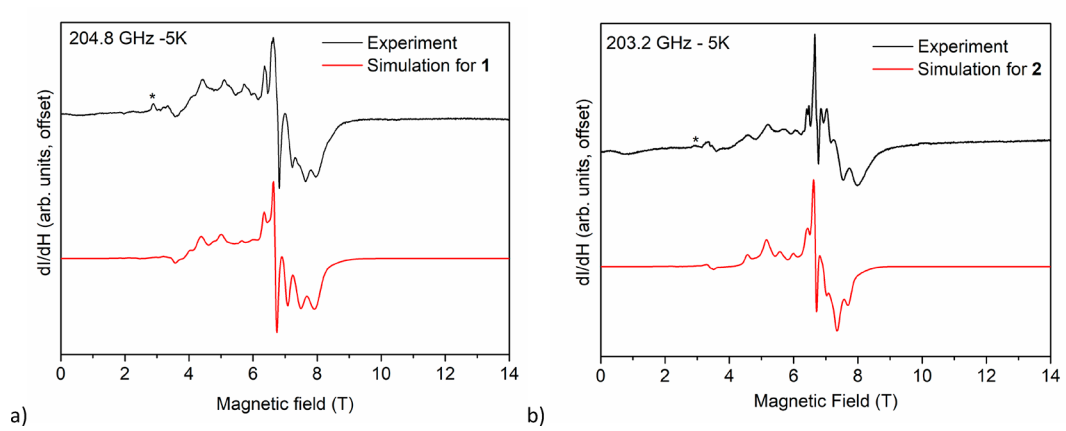

Figure 4. High-field powder EPR spectrum (in black) recorded at 5 K and 204.8 GHz for **1** (a) and 203.2 GHz for **2** (b). The simulated spectra (in red) are displayed below the experimental ones. It is apparent that three Ni_4 species with different ZFS parameters contribute to these spectra. To reflect this, the spectra simulated according to the parameters given in Table 3 were appropriately weighted and summed (in red). The features marked by (*) are due to surface adsorbed molecular oxygen. Details regarding the simulations are addressed in Figure S3.

Table 3. ZFS Parameters for the Three Species of Both Compounds, Including the Relative Weights Needed to Best Simulate the Powder EPR Spectra

	compound **1**				compound **2**			
	D_{mol} (cm^{-1})	g	weight (%)	D_{strain} (cm^{-1})	D_{mol} (cm^{-1})	g	weight (%)	D_{strain} (cm^{-1})
species 1	−0.33	2.22	24	0.04	−0.21	2.20	35	0.04
species 2	−0.38	2.22	8	0.03	−0.30	2.20	10	0.02
species 3	−0.27	2.22	68	0.14	−0.26	2.20	55	0.11

cm^{-1} to +7.59 cm^{-1}) typically observed for hexacoordinated Ni^{II} with an elongated distortion.[33,34,40−42]

For compound **1**, the ZFS term of the Hamiltonian described by eq 2 was slightly modified to take into account the different configuration of the hard axis alignment for the Ni4 ion, along the X axis instead of the Y axis (S^2_{4X} instead of S^2_{4Y} in eq 2) (see Figure 2(a)). The first attempt to fit the magnetic data allowed all parameters to vary and resulted in a very good fit. However, the obtained exchange coupling constants, $J_1 = J_2 \sim 9$ cm^{-1}, appear to be unphysical in spite of the differences in the Ni−O−Ni angles associated with the two exchange pathways. Additional attempts to account for the different exchange pathways with more than two coupling constants produced similar inconsistent results. Therefore, we decided to fix the value of J_1 to that obtained for compound **2**. The best fit is shown in Figure 3a with the following parameters: $g = 2.24 \pm 0.02$, $J_1 = -1.1$ cm^{-1} (fixed), $J_2 = 16.1 \pm 0.02$ cm^{-1}, and $D_{Ni^{II}} = 8.6 \pm 0.03$ cm^{-1}. These values are close to the values found in the literature for Ni^{II}- based cubanes.[39,8] The axial ZFS parameter $D_{Ni^{II}}$ is slightly altered depending on the fixed value of J_1 and is found to lie approximately between 6.5 and 8.5 cm^{-1}. Similarly, to compound **2**, the ground state corresponds to $S = 4$.

HFEPR Spectroscopy. We recorded powder HFEPR spectra for the two Ni-cubane complexes in the frequency range from 102.4 to 406.4 GHz, with temperature from 5 to 20 K. Representative spectra are shown in Figure 4. For both compounds, the previous analysis of the magnetic behavior described by the susceptibility data showed that the leading isotropic exchange interactions are ferromagnetic. Since the local ZFS associated with the Ni^{II} ions is weak in comparison with the dominant nearest neighbor exchange interaction, the HFEPR spectra can be well described on the basis of excitations within an isolated total spin $S_T = 4$ ground state multiplet, using the following spin-Hamiltonian:

$$\hat{H} = \mu_B g\vec{B}\cdot\hat{S} + D_{mol}\hat{S}_z^2 \quad (3)$$

where the first term represents the Zeeman interaction and the second term defines the second-order axial ZFS.

In order to obtain satisfactory simulations of the experimental EPR spectra according to eq 3, we found necessary to consider at least three distinct $S_T = 4$ Ni_4 species within the crystals of both compounds. The case for two species is quite apparent in the spectra of complex **1**, where one clearly sees a doubling of many of the EPR peaks. This doubling is captured by superimposing simulations with slightly different D_{mol} parameters and similar line widths. However, the best agreement is obtained by adding a third component with similar D_{mol} parameter but with a much larger line width (see also Figure S3). The broad signal is suggestive of significant disorder in the samples, while the sharper resolvable signals indicate discrete Ni_4 species. Disorder is unavoidable in molecular crystals. It is frequently caused by solvent loss and can be exacerbated by grinding crystals to form powder samples. Such disorder is invisible to bulk thermodynamic probes (e.g., $\chi_M T$ data) but is always very apparent in EPR (i.e., spectroscopic) measurements. Indeed, effects of disorder have previously been extensively studied among other families of Ni_4 clusters. The disorder gives rise to distributions (strains) in the molecular structural parameters and, hence, to distributions in ZFS parameters. It has additionally been shown that discrete disorder associated with different ligand group conformations may give rise to EPR peak splittings, i.e., resolvable multimodal distributions of ZFS parameters.[43−45] The observation of distinct species in compound **2** is not surprising given the two distinct molecules

DOI: 10.1021/acs.inorgchem.9b01816
Inorg. Chem. 2019, 58, 14420−14428

in the asymmetric unit. The explanation for compound **1** is less clear. However, as noted above, this could be due to a discrete disorder.

The relevant ZFS parameters of the three species used to simulate the EPR spectra of compounds **1** and **2** are summarized in Table 3. Here, the strain is parametrized by a Gaussian distribution of width defined in the D_{strain} column centered at the listed D_{mol} value. From Table 3, species 1 and 2 are responsible for the more prominent sharp resonances seen in Figure 4. These two slightly different values of D_{mol} were chosen to best replicate the resonance positions of the easy-(z) axis components of the powder spectra (the resonances on the low field side of the sharp g = 2.00 signal at ∼6.6 T). The third highly strained species then reproduces the underlying broad background. The total simulation is thus given by a weighted sum of all three parameter sets, with their respective weights summarized in Table 3. These simulations are included below the experimental spectra in Figure 4 (black = data, red = simulations); details regarding the summation of the simulations for the three species can be found in Figure S3.

Variable temperature measurements allow for the determination of the sign of the ZFS at low temperature; a negative D parameter will enhance the intensity in the extremities of the spectra, while the opposite will be observed for a complex with a positive D parameter. These temperature dependences are displayed in Figures S4 and S5 and demonstrate that the relative intensities of the spectra change markedly upon warming/cooling, confirming the negative signs of the D parameters. We note that the absolute values are also within the range observed for other tetranuclear ferromagnetically coupled Ni^{II}-based compounds.[7,37,30]

To corroborate the results from the HFEPR measurements, isothermal magnetization was measured as a function of applied magnetic field for both compounds (Figure S6). Since it was determined that the spin ground state corresponds to S_T = 4, the magnetic data were fitted with the same giant spin Hamiltonian as used to simulate the HFEPR spectra (eq 3). The best fits were obtained with g = 2.18 ± 0.02 and D_{mol} = −0.28 ± 0.10 cm^{-1} for **1** and with g = 2.19 ± 0.05 and D_{mol} = −0.35 ± 0.13 cm^{-1} for **2** and are quite consistent with the EPR results. It is known that an orthogonal hard-axis alignment in a S_4-symmetry spin cluster, as for **2** (Figure 3b), results in a negative molecular axial ZFS parameter.[46] In this configuration, the relation between the molecular and the local axial ZFS parameters can be approximated by the following expression:[35]

$$D_{mol} = -\frac{1}{14} D_{Ni^{II}} \quad (4)$$

By replacing the $D_{Ni^{II}}$ value obtained from the susceptibility data for complex **2** (+5.2 cm^{-1}) in eq 4, the calculated D_{mol} value is −0.37 cm^{-1}, which is in good accordance with the results obtained from the isothermal magnetization and HFEPR data.

The relation given by eq 4 does not explicitly apply to compound **1** since the local ZFS tensors are not in an orthogonal hard-axis arrangement as given by Figure 2b. However, in the high field limit, we find that the energy levels associated with the z components of the EPR spectra remain relatively unchanged, regardless of the orientation of the local "Ni4" ion. As such, the total molecular axial zero field splitting of compound **1** is well described by a D_{mol} value of similar magnitude to compound **2**. This relation does not hold for the xy components, as the orientation of the "Ni4" ion highlighted by the orange axis in Figure 2a breaks the ∼S_4 symmetry of compound **2**. However, due to the significant strain required to replicate the EPR data discussed above, the spectral features associated with any rhombicity in the ZFS cannot be easily resolved in either compound.

CONCLUSION

We report the synthesis, crystal structure, and magneto-structural correlation of two tetranuclear Ni^{II} complexes. Our synthetic approach leads to the tetranuclear species, despite the difference in the basicity of the β-diketonate ligand and using milder conditions than other compounds with a Ni_4O_4 core. Surprisingly, the use of different β-diketonate ligands contributed to a different arrangement of the hard-axes of the Ni^{II} ions in the cubane clusters. To the best of our knowledge, these are two of a few examples of Ni_4-based cubanes with β-diketonate ligands, since most of the compounds reported in the literature contain a Schiff base as the ligands. The analysis of the magnetic susceptibility data shows that ferromagnetic interactions are predominant in these compounds. The magnitude and sign of the obtained axial ZFS parameter for each Ni^{II} ion lies within the range (from +0.9 cm^{-1} to +7.59 cm^{-1}) typically observed for hexacoordinated Ni^{II} with an elongated distortion. HFEPR measurements confirm the expected S_T = 4 spin ground states and the negative magnetocrystalline anisotropy (D_{mol} < 0) for both compounds. An unusual splitting of the EPR peaks may, in some cases, be interpreted in terms of distinct Ni_4 species within the crystals.

ASSOCIATED CONTENT

Supporting Information

The Supporting Information is available free of charge on the ACS Publications website at DOI: 10.1021/acs.inorgchem.9b01816.

Experimental and simulated powder X-ray diffraction (PXRD) (Figure S1); ORTEP representation of the asymmetric units of compounds **1** and **2** (Figure S2); selected bond lengths and angles for **1** and **2** (Table S1); details about the spectral simulations of the powder EPR spectra and the temperature-dependent powder EPR spectra for both compounds (Figures S3−S5); and the isothermal magnetization M versus H/T curves measured at 1.8, 4, and 8 K for both compounds (Figure S6) (PDF)

Accession Codes

CCDC 1903092 and 1903630 contain the supplementary crystallographic data for this paper. These data can be obtained free of charge via www.ccdc.cam.ac.uk/data_request/cif, or by emailing data_request@ccdc.cam.ac.uk, or by contacting The Cambridge Crystallographic Data Centre, 12 Union Road, Cambridge CB2 1EZ, UK; fax: +44 1223 336033.

AUTHOR INFORMATION

Corresponding Authors

*E-mail: mgfvaz@gmail.com (M.G.F.V.).
*E-mail: shill@magnet.fsu.edu (S.H.).

ORCID

Lívia B. L. Escobar: 0000-0001-8899-0261
Guilherme P. Guedes: 0000-0001-6138-9943

DOI: 10.1021/acs.inorgchem.9b01816
Inorg. Chem. 2019, 58, 14420−14428

Stéphane Soriano: 0000-0002-5577-1086
Stephen Hill: 0000-0001-6742-3620
Maria G. F. Vaz: 0000-0001-9855-5909

Notes

The authors declare no competing financial interest.

■ ACKNOWLEDGMENTS

The authors are thankful for the financial support provided by the Brazilian agencies FAPERJ and CNPq. We also acknowledge LabCri-UFMG (Brazil) and LDRX-UFF for use of their laboratory facilities. The authors are thankful for support from the Coordenação de Aperfeiçoamento de Pessoal de Nível Superior, Brazil, (CAPES) within the scope of the Capes-PrInt Program, Financial Code 001, project number 88887.310269/2018-00. L.B.L.E. acknowledges CAPES for the fellowship that allowed part of this work to be performed at the NHMFL-USA. S.H. acknowledges the support of the U.S. National Science Foundation (DMR-1610226). Work performed at the NHMFL is supported by the NSF (DMR-1157490) and the State of Florida.

■ REFERENCES

(1) Lis, T. Preparation, Structure, and Magnetic Properties of a Dodecanuclear Mixed-valence Manganese Carboxylate. *Acta Crystallogr., Sect. B: Struct. Crystallogr. Cryst. Chem.* **1980**, *36*, 2042−2046.
(2) Sessoli, R.; Gatteschi, D.; Caneschi, A.; Novak, M. A. Magnetic Bistabilitiy in a Metal-Ion Cluster. *Nature* **1993**, *365* (6176), 141−143.
(3) Bar, A. K.; Kalita, P.; Singh, M. K.; Rajaraman, G.; Chandrasekhar, V. Low-Coordinate Mononuclear Lanthanide Complexes as Molecular Nanomagnets. *Coord. Chem. Rev.* **2018**, *367*, 163−216.
(4) Chakraborty, A.; Goura, J.; Kalita, P.; Swain, A.; Rajaraman, G.; Chandrasekhar, V. Heterometallic 3d-4f Single Molecule Magnets Containing Diamagnetic Metal Ions. *Dalt. Trans.* **2018**, *47* (27), 8841−8864.
(5) Gaita-Ariño, A.; Luis, F.; Hill, S.; Coronado, E. Molecular Spins for Quantum Computation. *Nat. Chem.* **2019**, *11* (4), 301−309.
(6) Ponomaryov, A. N.; Kim, N.; Hwang, J.; Nojiri, H.; Van Tol, J.; Ozarowski, A.; Park, J.; Jang, Z.; Suh, B.; Yoon, S.; Choi, K. Structural Tailoring Effects on the Magnetic Behavior of Symmetric and Asymmetric Cubane-Type Ni Complexes. *Chem. - Asian J.* **2013**, *8* (6), 1152−1159.
(7) Aromí, G.; Bouwman, E.; Burzurí, E.; Carbonera, C.; Krzystek, J.; Luis, F.; Schlegel, C.; Van Slageren, J.; Tanase, S.; Teat, S. J. A Novel Ni4 Complex Exhibiting Microsecond Quantum Tunneling of the Magnetization. *Chem. - Eur. J.* **2008**, *14* (35), 11158−11166.
(8) Herchel, R.; Nemec, I.; Machata, M.; Trávníček, Z. Solvent-Induced Structural Diversity in Tetranuclear Ni(II) Schiff-Base Complexes: The First Ni4 Single-Molecule Magnet with a Defective Dicubane-like Topology. *Dalt. Trans.* **2016**, *45* (46), 18622−18634.
(9) Ferguson, A.; Lawrence, J.; Parkin, A.; Sanchez-Benitez, J.; Kamenev, K. V.; Brechin, E. K.; Wernsdorfer, W.; Hill, S.; Murrie, M. Synthesis and Characterisation of a Ni4 Single-Molecule Magnet with S4 Symmetry. *J. Chem. Soc. Dalt. Trans.* **2008**, *45*, 6409−6414.
(10) Torić, F.; Pavlović, G.; Pajić, D.; Cindrić, M.; Zadro, K. Tetranuclear Ni4 Cubane Complexes with High XT Maxima: Magneto-Structural Analysis. *CrystEngComm* **2018**, *20* (27), 3917−3927.
(11) De Souza, M. S.; Briganti, M.; Reis, S. G.; Stinghen, D.; Bortolot, C. S.; Cassaro, R. A. A.; Guedes, G. P.; Da Silva, F. C.; Ferreira, V. F.; Novak, M. A.; et al. Magnetic Cationic Copper(II) Chains and a Mononuclear Cobalt(II) Complex Containing $[Ln(Hfac)_4]^-$ Blocks as Counterions. *Inorg. Chem.* **2019**, *58* (3), 1976−1987.
(12) Guedes, G. P.; Soriano, S.; Comerlato, N. M.; Speziali, N. L.; Lahti, P. M.; Novak, M. A.; Vaz, M. G. F. Two Cobalt(II) Cubane Compounds: The Key Role of Small Ligand Changes on the Crystal Packing and Magnetic Properties. *Eur. J. Inorg. Chem.* **2012**, *2012* (34), 5642−5648.
(13) Guedes, G. P.; Soriano, S.; Comerlato, N. M.; Speziali, N. L.; Novak, M. A.; Vaz, M. G. F. Heptanuclear Cobalt(II) Dicubane Compounds with Single-Molecule Magnet Behavior. *Inorg. Chem. Commun.* **2013**, *37*, 101−105.
(14) Lawrence, J.; Yang, E. C.; Edwards, R.; Olmstead, M. M.; Ramsey, C.; Dalal, N. S.; Gantzel, P. K.; Hill, S.; Hendrickson, D. N. Disorder and Intermolecular Interactions in a Family of Tetranuclear Ni(II) Complexes Probed by High-Frequency Electron Paramagnetic Resonance. *Inorg. Chem.* **2008**, *47* (6), 1965−1974.
(15) Krzystek, J.; Ozarowski, A.; Telser, J. Multi-Frequency, High-Field EPR as a Powerful Tool to Accurately Determine Zero-Field Splitting in High-Spin Transition Metal Coordination Complexes. *Coord. Chem. Rev.* **2006**, *250* (17−18), 2308−2324.
(16) Escobar, L. B. L.; Guedes, G. P.; Soriano, S.; Cassaro, R. A. A.; Marbey, J.; Hill, S.; Novak, M. A.; Andruh, M.; Vaz, M. G. F. Synthesis, Crystal Structures, and EPR Studies of First $Mn^{III}Ln^{III}$ Hetero-Binuclear Complexes. *Inorg. Chem.* **2018**, *57* (1), 326−334.
(17) *CrysAlis RED*, version 1.171.32.3; Oxford Diffraction Ltd.: Abingdon, U.K., 2008.
(18) Hooft, R. W. *COLLECT*; Nonius BV: Delft, The Netherlands, 1998.
(19) Otwinowski, Z.; Minor, W. *DENZO/SCALEPACK*; Academic Press: New York, 1997; pp 307−326.
(20) Blessing, R. H. An Empirical Correction for Absorption Anisotropy. *Acta Crystallogr., Sect. A: Found. Crystallogr.* **1995**, *51*, 33.
(21) Sheldrick, G. M. A Short History of SHELX. *Acta Crystallogr., Sect. A: Found. Crystallogr.* **2008**, *A64*, 112−122.
(22) Farrugia, L. J. ORTEP-3 for Windows - a Version of ORTEP-III with a Graphical User Interface (GUI). *J. Appl. Crystallogr.* **1997**, *30*, 565.
(23) Momma, K.; Izumi, F. VESTA 3 for Three-Dimensional Visualization of Crystal, Volumetric and Morphology Data. *J. Appl. Crystallogr.* **2011**, *44* (6), 1272−1276.
(24) Bain, G. A.; Berry, J. F. Diamagnetic Corrections and Pascal's Constants. *J. Chem. Educ.* **2008**, *85* (4), 532−536.
(25) Hassan, A. K.; Pardi, L. A.; Krzystek, J.; Sienkiewicz, A.; Goy, P.; Rohrer, M.; Brunel, L. C. Ultrawide Band Multifrequency High-Field EMR Technique: A Methodology for Increasing Spectroscopic Information. *J. Magn. Reson.* **2000**, *142*, 300−312.
(26) Stoll, S.; Schweiger, A. EasySpin, a Comprehensive Software Package for Spectral Simulation and Analysis in EPR. *J. Magn. Reson.* **2006**, *178*, 42−55.
(27) Kessler, V. G.; Gohil, S.; Kritikos, M.; Korsak, O. N.; Knyazeva, E. E.; Moskovskaya, I. F.; Romanovsky, B. V. An Approach to Heterometallic Alkoxide-β-Diketonate Complexes with a M_4O_4 Cubane-like Core and New Prospects of Their Application in Preparation of Solid Catalysts. X-Ray Single Crystal Study of $(Co,Ni)_4(Acac)_4(\mu_3\text{-}OMe)_4(MeOH)_4$. *Polyhedron* **2001**, *20* (9−10), 915−922.
(28) Guedes, G. P.; Junior, H. C. S.; Vaz, M. G. F. New Step-by-Step Hexanuclear Copper(II) Compound: Synthesis, Crystal Structure and Magnetic Properties. *Inorg. Chem. Commun.* **2017**, *86*, 62−65.
(29) Berry, J. F.; Cotton, F. A.; Liu, C. Y.; Lu, T.; Murillo, C. A.; Tsukerblat, B. S.; Villagrán, D.; Wang, X. Modeling Spin Interactions in a Cyclic Trimer and a Cuboidal Co_4O_4 Core with Co(II) in Tetrahedral and Octahedral Environments. *J. Am. Chem. Soc.* **2005**, *127*, 4895−4902.
(30) Petit, S.; Neugebauer, P.; Pilet, G.; Chastanet, G.; Barra, A.-L.; Antunes, A. B.; Wernsdorfer, W.; Luneau, D. Condensation of a Nickel Tetranuclear Cubane into a Heptanuclear Single-Molecule Magnet. *Inorg. Chem.* **2012**, *51*, 6645−6654.
(31) Halcrow, M. A.; Sun, J.-S.; Huffman, J. C.; Christou, G. Structural and Magnetic Properties of $[Ni_4(\mu_3\text{-}OMe)_4(dbm)_4(MeOH)_4]$ and $[Ni_4(\eta^1,\mu_3\text{-}N_3)_4(dbm)_4(EtOH)_4]$.

DOI: 10.1021/acs.inorgchem.9b01816
Inorg. Chem. 2019, 58, 14420−14428

Magnetostructural Correlations for $[Ni_4X_4]^{4+}$ Cubane Complexes. *Inorg. Chem.* **1995**, *34* (16), 4167−4177.
(32) Titiš, J.; Boča, R. Magnetostructural D Correlations in Hexacoordinated Cobalt(II) Complexes. *Inorg. Chem.* **2011**, *50* (22), 11838−11845.
(33) Mašlejová, A.; Ivaniková, R.; Svoboda, I.; Papánková, B.; Dlháň, L.; Mikloš, D.; Fuess, H.; Boča, R. Structural Characterization and Magnetic Properties of Hexakis(Imidazole)Nickel(II) Bis(Formate), Bis(Chloroacetate), Bis(2-Chloropropionate) and Hexakis(1-Methyl-Imidazole)Nickel(II) Chloride Dihydrate. *Polyhedron* **2006**, *25* (8), 1823−1830.
(34) Titiš, J.; Boča, R. Magnetostructural D Correlation in Nickel(II) Complexes: Reinvestigation of the Zero-Field Splitting. *Inorg. Chem.* **2010**, *49* (9), 3971−3973.
(35) Sieber, A.; Boskovic, C.; Bircher, R.; Waldmann, O.; Ochsenbein, S. T.; Chaboussant, G.; Güdel, H. U.; Kirchner, N.; Van Slageren, J.; Wernsdorfer, W.; et al. Synthesis and Spectroscopic Characterization of a New Family of Ni4 Spin Clusters. *Inorg. Chem.* **2005**, *44* (12), 4315−4325.
(36) Yang, E. C.; Wernsdorfer, W.; Hill, S.; Edwards, R. S.; Nakano, M.; Maccagnano, S.; Zakharov, L. N.; Rheingold, A. L.; Christou, G.; Hendrickson, D. N. Exchange Bias in Ni4 Single-Molecule Magnets. *Polyhedron* **2003**, *22* (14−17), 1727−1733.
(37) Iasco, O.; Chumakov, Y.; Guégan, F.; Gillon, B.; Lenertz, M.; Bataille, A.; Jacquot, J.-F.; Luneau, D. Mapping the Magnetic Anisotropy inside a Ni4 Cubane Spin Cluster Using Polarized Neutron Diffraction. *Magnetochemistry* **2017**, *3* (3), 25.
(38) Azuah, L. R.; Qiu, Y.; Tregenna-Piggott, P. L. W.; Brown, C. M.; Copley, J. R. D.; Dimeo, R. M.; Kneller, L. R. DAVE: A Comprehensive Software Suite for the Reduction, Visualization, and Analysis of Low Energy Neutron Spectroscopic Data. *J. Res. Natl. Inst. Stand. Technol.* **2009**, *114*, 341−358.
(39) Das, M.; Herchel, R.; Trávníček, Z.; Bertolasi, V.; Ray, D. Anion Coordination Directed Synthesis Patterns for [Ni4] Aggregates: Structural Changes for Thiocyanate Coordination and Ligand Arm Hydrolysis. *New J. Chem.* **2018**, *42* (20), 16717−16728.
(40) Packová, A.; Miklovič, J.; Titiš, J.; Koman, M.; Boča, R. Positive Zero-Field Splitting in a Hexacoordinate Nickel(II) Complex. *Inorg. Chem. Commun.* **2013**, *32*, 9−11.
(41) Dobrzynska, D.; Jerzykiewicz, L. B.; Duczmal, M.; Wojciechowska, A.; Jabłonska, K.; Palus, J.; Ozarowski, A. Structural, Spectroscopic, and Magnetic Study of Bis(9,10-Dihydro-9-Oxo-10-Acridineacetate)Bis(Imidazole)Bis(Methanol) Nickel(II). *Inorg. Chem.* **2006**, *45* (26), 10479−10486.
(42) Pladzyk, A.; Ozarowski, A.; Ponikiewski, Ł. Crystal and Electronic Structures of Ni(II) Silanethiolates Containing Flexible Diamine Ligands. *Inorg. Chim. Acta* **2016**, *440*, 84−93.
(43) Hill, S. Magnetization Tunneling in High-Symmetry Mn_{12} Single-Molecule Magnets. *Polyhedron* **2013**, *64*, 128−135.
(44) Maccagnano, S.; Yang, E.-C.; Hill, S.; Edwards, R. S.; Wernsdorfer, W.; Christou, G.; Hendrickson, D. High-Frequency Electron Paramagnetic Resonance Investigations of Tetranuclear Nickel-Based Single-Molecule Magnets. *J. Appl. Phys.* **2003**, *93* (10), 7807−7809.
(45) Liu, J.; Hill, S. Magnetization Quantum Tunneling and Improper Rotational Symmetry. *Polyhedron* **2013**, *66*, 147−152.
(46) Nakano, M.; Matsubayashi, G.-E.; Muramatsu, T.; Kobayashi, T. C.; Amaya, K.; Yoo, J.; Christou, G.; Hendrickson, D. N. Slow Magnetization Reversal in $[Ni_4(OMe)_4(Sal)_4(MeOH)_4]$. *Mol. Cryst. Liq. Cryst.* **2002**, *376*, 405−410.

DOI: 10.1021/acs.inorgchem.9b01816
Inorg. Chem. 2019, 58, 14420−14428